Cite as: J. Terreros-Roncal *et al*., *Science* 10.1126/science.abl5163 (2021).

Impact of neurodegenerative diseases on human adult hippocampal neurogenesis

J. Terreros-Roncal[1,2,3]†, E. P. Moreno-Jiménez[1,2,3]†, M. Flor-García[1,2,3]†, C. B. Rodríguez-Moreno[1,3], M. F. Trinchero[4], F. Cafini[5], A. Rábano[6], M. Llorens-Martín[1,3]*

[1]Department of Molecular Neuropathology, Centro de Biología Molecular "Severo Ochoa" (CBMSO), Spanish Research Council (CSIC)–Universidad Autónoma de Madrid (UAM), Madrid, Spain. [2]Department of Molecular Biology, Faculty of Sciences, Universidad Autónoma de Madrid, Madrid, Spain. [3]Center for Networked Biomedical Research on Neurodegenerative Diseases (CIBERNED), Madrid, Spain.[4]Laboratory of Neuronal Plasticity, Leloir Institute (IIBBA - CONICET); Buenos Aires, Argentina.[5]Universidad Europea de Madrid, Faculty of Biomedical and Health Sciences, Madrid, Spain. [6]Neuropathology Department, CIEN Foundation, Madrid, Spain.

†These authors contributed equally to this work.

*Corresponding author. Email: m.llorens@csic.es

Disrupted hippocampal performance underlies psychiatric comorbidities and cognitive impairment in patients with neurodegenerative disorders. To understand the contribution of adult hippocampal neurogenesis (AHN) to Amyotrophic lateral sclerosis, Huntington's disease, Parkinson's disease, dementia with Lewy bodies, and Frontotemporal dementia, we studied post-mortem human samples. We found that adult-born dentate granule cells showed abnormal morphological development and changes in the expression of differentiation markers. The ratio of quiescent to proliferating hippocampal neural stem cells was shifted and the homeostasis of the neurogenic niche, altered. Aging and neurodegenerative diseases reduced the phagocytic capacity of microglia, triggered astrogliosis, and altered the microvasculature of the dentate gyrus. Thus, enhanced vulnerability of AHN to neurodegeneration might underlie hippocampal dysfunction during physiological and pathological aging in humans.

The addition of new neurons to the hippocampus throughout life—a process known as adult hippocampal neurogenesis (AHN) (*1*, *2*)—boosts hippocampal plasticity. AHN participates in mood regulation (*3*) and pattern separation (*4*). While exhaustively studied in rodents (*1*) and Old-World primates (*5*), this phenomenon has not been fully characterized in humans. The increased plasticity of the hippocampus seems to act as a double-edged sword, as this brain region also shows enhanced vulnerability to neurodegeneration. In fact, while the hippocampus is not the most affected brain region, impairments in this structure are believed to underlie the cognitive decline and the psychiatric symptoms observed in patients with various neurodegenerative diseases. Given the poorly characterized association between AHN and hippocampal dysfunction in our species, we sought to determine whether the dentate gyrus (DG) homeostasis and AHN dynamics show increased vulnerability to distinct forms of neurodegeneration.

AHN in neurologically healthy control subjects

To assess the presence of all the elements encompassed by AHN throughout human life, we examined a cohort of neurologically healthy control subjects (Fig. 1 and fig. S1 to S7). Previous studies identified immature dentate granule cells (DGCs) in the human DG (*6*–*9*), yet the presence of radial glia-like (RGL) cells with neural stem cell (NSC) properties (*10*) remains elusive. By subjecting high-quality post-mortem human samples to state-of-the-art tissue preservation methodologies (*6*), we identified a population of Nestin$^+$ cells that do not express S100β$^-$ (Fig. 1C and fig. S3) but other RGL markers, such as SRY-box 2 (Sox2), Vimentin, and glial fibrillary acidic protein (GFAP) (Fig. 1, A and D). Unlike Nestin$^+$ S100β$^+$ cells, Nestin$^+$ S100β$^-$ RGL cells show morphological characteristics of NSCs (e.g., long apical processes and of their cell bodies predominant distribution in the subgranular zone (SGZ)) (fig. S3). Phospho-Histone 3 (PH3)$^+$ proliferative cells and HuC/HuD$^+$ proliferative neuroblasts were also detected in the SGZ (Fig. 1, B and D, and fig. S4). The presence of these cells supports the notion that the human hippocampal NSC pool is preserved throughout life. These data are in agreement with the identification (using single-cell RNAseq) of a cluster of human DGCs proposed to represent precursor granule cells with neurogenic capacity (*11*), and they are compatible with the activation of quiescence mechanisms to maintain the proliferative capacity of NSCs and prevent their depletion (*12*).

Immature DGCs express the microtubule-associated protein Doublecortin (DCX) and go through various differentiation stages before becoming fully mature (*7*) (fig. S2G). Although DCX and Polysialylated-neural cell adhesion molecule (PSA-NCAM) are considered equivalent as markers of immature neurons in the adult brain, the expression of the latter slightly precedes that of the former during human AHN (fig. S2, A to G). DCX is not expressed by astrocytes, microglia, vascular structures, or interneurons (fig. S5, A to F). In contrast, DCX$^+$ DGCs express Prox1 (Fig. 1E and fig. S2I) and other neuronal markers that characterize distinct DGC maturation stages (*7*), including proliferative neuroblasts

(HuC/HuD), immature [PSA-NCAM, Calretinin (CR), or β-III Tubulin] and more differentiated DGCs (Neuronal nuclei (NeuN), Microtubule-associated protein 2 (MAP-2), three-repeated Tau (3R-Tau), and Calbindin (CB) (Fig. 1E and figs. S2J and S4A). Not only the expression of these markers varies during DGC maturation but also the cell positioning (Fig. 1, F and G), the presence (Fig. 1, F and H) and orientation (Fig. 1, F and I) of neurites, and the cell area (Fig. 1J and fig. S2H) become modified. In this regard, the most immature DCX^+ CR^+ DGCs are located at the SGZ, are small, and have various primary apical neurites horizontally oriented (*7*). In contrast, more differentiated DCX^+ CB^+ DGCs occupy upper positions in the granule cell layer (GCL) (fig. S2J), are larger, and have a single primary apical neurite oriented toward the molecular layer (*7*). Lastly, DCX^+ $NeuN^+$ DGCs show an intermediate state of maturation (Fig. 1, G to J, and fig. S2H), thereby supporting the dynamic nature of AHN in humans (fig. S2G).

AHN is orchestrated by the astrocytes (*13*), microglia (*14*) and vasculature (*15*) of the DG neurogenic niche in rodents, although the composition of a putatively equivalent structure in our species remains poorly characterized. We observed abundant astrocytes (Fig. 1, K and L) and microglia (Fig. 1, L to N), as well as a profuse network of *Ulex Europaea* Agglutinin 1 (UEA-1)$^+$ capillaries that occupied ~7% of the human GCL surface (Fig. 1O and fig. S2L) and were close to immature DGCs and RGL cells. Our observations reveal the cellular composition of the human DG neurogenic niche and also the remodeling of this niche throughout aging. Among the distinct components of this niche, microglia regulate AHN by controlling newborn neuron maturation (*14*). The former cells exhibit specialized membranous structures named phagocytic pouches, which allow them to phagocytose dysfunctional cells (*14*) (Fig. 1, M and N). The presence of such structures defines distinct morphological phenotypes in human microglia (fig. S6) and determines their phagocytic capacity, or *Phagocytic index* in mice (Fig. 1N and fig. S6F) (*14*), suggesting they may have similar functions in humans. Microglia lacking phagocytic pouches showed long nonpolarized processes, while the presence of these structures is accompanied by polarized morphologies and profusely branched processes. We observed a reduced number of phagocytic pouches in aged subjects (fig. S2M), thus pointing to a partially dysfunctional microglial phenotype and suggesting that altered microglial function is one of the mechanisms underpinning the age-associated AHN decline in our species.

AHN in neurodegenerative diseases

Given the reduction of AHN during physiological aging, we questioned whether this phenomenon was also compromised by distinct forms of neurodegeneration. AHN is altered in mouse models of Amyotrophic lateral sclerosis (ALS) (*16*). In the light of the hippocampal alterations (*17*) and the increased density of pyknotic cells (fig. S8C) found in the DG of patients with ALS, we first assessed the vulnerability of AHN to this disorder (Fig. 2 and figs. S1 and S9). The densities of $PH3^+$ and HuC/HuD^+ cells remained unchanged (Fig. 2, C and E, and fig. S9A), thereby indicating that proliferation was preserved in these patients. In contrast, they showed increased densities of NSCs (Fig. 2, A, B, D, and E) and DCX^+ immature DGCs (Fig. 2, F to I, and fig. S9, B to E), although the morphological development of the latter tended to be impaired (Fig. 2, I to K). Subsequently, we examined the integrity of the DG neurogenic niche and observed DG astrogliosis (Fig. 2, L and M) and a reduced number of microglial phagocytic pouches (Fig. 2N). Moreover, DG capillaries tended to be thicker (Fig. 2P and fig. S9N). Taken together, these results indicate that both AHN and the homeostasis of the DG neurogenic niche are vulnerable to ALS. The AHN phenotype observed in these patients was characterized by increased numbers of RGL cells and immature DGCs that tended to be morphologically aberrant.

Hippocampal alterations (*18*) are believed to underlie the early spatial learning deficits observed in patients with Huntington's disease and are consistent with the presence of mutant Huntingtin and the increased density of pyknotic nuclei observed in the DG of these patients (figs. S10N and S8D). Therefore, we studied the targeting of AHN by Huntington's disease (Figs. 3, S1, and S10). The densities of $Nestin^+$ $S100\beta^-$ NSCs (Fig. 3, A and D) and immature DGCs (Fig. 3, F and G) were increased in patients with this disorder, while that of $Sox2^+$ and proliferative cells (Fig. 3, B, C, and E) remained unchanged. Immature DGCs showed early maturation impairments (Fig. 3H), possibly related to their lengthened initial differentiation stages (Fig. 3I and fig. S10, L and M), morphological abnormalities (Fig. 3, L to N, and fig. S10, B and C), and reduced NeuN expression (Fig. 3H), which is in agreement with results obtained from mouse models (*19*). The homeostasis of the DG neurogenic niche was also affected (Fig. 3, O to S, and fig. S10, F to K), as suggested by the presence of DG astrogliosis (Fig. 3O), microglial alterations (reduced *Phagocytic index*, number of phagocytic pouches (Fig. 3, P to R), and nucleus area (fig. S10I)), and increased capillary thickness (Fig. 3S and fig. S10K). These results reveal the vulnerability of AHN and DG homeostasis to Huntington's disease. In patients with this condition, newborn DGCs showed early and late maturation impairments that led to their retention at undifferentiated stages.

α-synucleinopathies are characterized by the accumulation of α-synuclein aggregates in the brain. This family of disorders presents diverse clinical manifestations, including a variable temporal sequence of cognitive and motor impairments (*20*). We examined the integrity of AHN in two of these disorders, specifically Parkinson's disease (PD) and dementia with Lewy bodies (LD) (Fig. 4 and figs. S1, S11, and S12). Patients with these diseases showed an increased density of RGL cells (Fig. 4, A, B, E, and F) and morphological abnormalities in DCX^+ DGCs (Fig. 4, L and M, and figs. S11, E and F). However, other aspects of AHN seemed to be differentially altered in both conditions. Patients with PD showed increased densities of HuC/HuD^+ proliferative

neuroblasts and DCX$^+$ immature DGCs (data S1), which presented reduced expression of NeuN (data S1). We observed increased densities of pyknotic cells (fig. S8E), compromised microglial phagocytic capacity (reduced *Phagocytic index* and nucleus area) (Fig. 4, O to Q), and increased DG capillary thickness (Fig. 4, R and S, and fig. S11M) in both α-synucleinopathies. Patients with PD also presented DG astrogliosis, which indicates a more severe alteration in the integrity of the DG neurogenic niche (data S1). All together, these results reveal that these two α-synucleinopathies differentially target the DG milieu and generate singular AHN signatures (data S1). While patients with PD presented a generalized increase in several neurogenic cell populations, which also showed maturation impairments, those with LD showed milder alterations in all the aforementioned stages of AHN and the DG neurogenic niche.

In line with the diffuse degeneration of the frontal and temporal lobes of their brain (*21*), patients with Frontotemporal dementia (FTD) also showed mild AHN alterations (Fig. 5 and figs. S1 and S13). They presented unchanged densities of NSCs (Fig. 5, C and D, and fig. S13, A and B) and of immature DGCs (Fig. 5E and fig. S13, C to E), reduced densities of HuC/HuD$^+$ proliferative neuroblasts (Fig. 5, B and D), and moderately impaired DGC differentiation (Fig. 5, F to J, and fig. S13F). Mild signs of disturbed DG homeostasis (Fig. 5, K to O), such as increased density of pyknotic cells (fig. S8F), astrogliosis (Fig. 5, K and L), increased capillary thickness (Fig. 5O and fig. S13O), and a trend to reduced microglial *Phagocytic index* (Fig. 5M and N), were also observed. These results reveal that FTD moderately targets AHN by causing an imbalance in the RGL/proliferative cell ratio, triggering the presence of morphologically aberrant DGCs, and altering the DG neurogenic niche homeostasis.

Our data reveal the vulnerability of human AHN to distinct neurodegenerative diseases. The heterogeneous nature of the hippocampal alterations in patients with ALS (*22*), Huntington's disease (*23*), α-synucleinopathies (*20*, *24*), and FTD (*21*) is likely to underlie the specific disease-associated AHN signatures observed (Fig. 6 and data S1). The imbalanced number of RGL and proliferative cells noted in patients with ALS, Huntington's disease, LD, and FTD point to enhanced quiescence of the former cells or to impaired survival of their immediate progeny, thus suggesting selective vulnerability of RGL and proliferative cells to certain disorders. In contrast, other aspects of AHN, such as DGC maturation, were affected in all the diseases studied and might be caused by the global disruption of DG homeostasis. In addition to local pathological effects, the neurodegeneration of other brain areas primarily affected by these conditions might alter the DG homeostasis through long-distance signaling mechanisms. In this regard, the observed increase in DG vascularization might either exert neuroprotective effects or amplify the detrimental consequences of local and disstal neuroinflammation, thereby contributing to the progressive impairment of microglial functions. The reduction of microglial phagocytic capacity correlates with the number of DG pyknotic cells and the severity of AHN impairments in patients with ALS, Huntington's disease, and α-synucleinopathies. Moreover, impaired microglial phagocytosis triggers astrogliosis (*25*), a phenomenon evident in all the diseased individuals studied here. Therefore, the generalized alteration of DG homeostasis might be a direct pathway through which neurodegenerative diseases target AHN dynamics in our species.

AHN is crucial in learning, memory, and mood regulation. In fact, failure of AHN is related to memory deficits in humans (*8*, *26*). Our results point to AHN impairment as a mechanism underlying hippocampal dysfunction in aged and diseased subjects. Unraveling the complex crosstalk established between the elements that make up the human DG neurogenic niche and AHN dynamics is expected to improve our understanding of the physiological roles played by AHN, which functions as a lifelong reserve of plasticity in the human brain.

REFERENCES AND NOTES

1. J. Altman, Autoradiographic investigation of cell proliferation in the brains of rats and cats. *Anat. Rec.* **145**, 573–591 (1963). doi:10.1002/ar.1091450409 Medline

2. P. S. Eriksson, E. Perfilieva, T. Björk-Eriksson, A. M. Alborn, C. Nordborg, D. A. Peterson, F. H. Gage, Neurogenesis in the adult human hippocampus. *Nat. Med.* **4**, 1313–1317 (1998). doi:10.1038/3305 Medline

3. A. S. Hill, A. Sahay, R. Hen, Increasing Adult Hippocampal Neurogenesis is Sufficient to Reduce Anxiety and Depression-Like Behaviors. *Neuropsychopharmacology* **40**, 2368–2378 (2015). doi:10.1038/npp.2015.85 Medline

4. A. Sahay, K. N. Scobie, A. S. Hill, C. M. O'Carroll, M. A. Kheirbek, N. S. Burghardt, A. A. Fenton, A. Dranovsky, R. Hen, Increasing adult hippocampal neurogenesis is sufficient to improve pattern separation. *Nature* **472**, 466–470 (2011). doi:10.1038/nature09817 Medline

5. E. Gould, A. J. Reeves, M. Fallah, P. Tanapat, C. G. Gross, E. Fuchs, Hippocampal neurogenesis in adult Old World primates. *Proc. Natl. Acad. Sci. U.S.A.* **96**, 5263–5267 (1999). doi:10.1073/pnas.96.9.5263 Medline

6. M. Flor-García, J. Terreros-Roncal, E. P. Moreno-Jiménez, J. Ávila, A. Rábano, M. Llorens-Martín, Unraveling human adult hippocampal neurogenesis. *Nat. Protoc.* **15**, 668–693 (2020). doi:10.1038/s41596-019-0267-y Medline

7. E. P. Moreno-Jiménez, M. Flor-García, J. Terreros-Roncal, A. Rábano, F. Cafini, N. Pallas-Bazarra, J. Ávila, M. Llorens-Martín, Adult hippocampal neurogenesis is abundant in neurologically healthy subjects and drops sharply in patients with Alzheimer's disease. *Nat. Med.* **25**, 554–560 (2019). doi:10.1038/s41591-019-0375-9 Medline

8. M. K. Tobin, K. Musaraca, A. Disouky, A. Shetti, A. Bheri, W. G. Honer, N. Kim, R. J. Dawe, D. A. Bennett, K. Arfanakis, O. Lazarov, Human Hippocampal Neurogenesis Persists in Aged Adults and Alzheimer's Disease Patients. *Cell Stem Cell* **24**, 974–982.e3 (2019). doi:10.1016/j.stem.2019.05.003 Medline

9. M. Boldrini, C. A. Fulmore, A. N. Tartt, L. R. Simeon, I. Pavlova, V. Poposka, G. B. Rosoklija, A. Stankov, V. Arango, A. J. Dwork, R. Hen, J. J. Mann, Human Hippocampal Neurogenesis Persists throughout Aging. *Cell Stem Cell* **22**, 589–599.e5 (2018). doi:10.1016/j.stem.2018.03.015 Medline

10. B. Seri, J. M. García-Verdugo, B. S. McEwen, A. Alvarez-Buylla, Astrocytes give

rise to new neurons in the adult mammalian hippocampus. *J. Neurosci.* **21**, 7153–7160 (2001). doi:10.1523/JNEUROSCI.21-18-07153.2001 Medline

11. F. Ayhan, A. Kulkarni, S. Berto, K. Sivaprakasam, C. Douglas, B. C. Lega, G. Konopka, Resolving cellular and molecular diversity along the hippocampal anterior-to-posterior axis in humans. *Neuron* **109**, 2091–2105.e6 (2021). doi:10.1016/j.neuron.2021.05.003 Medline

12. L. Harris, P. Rigo, T. Stiehl, Z. B. Gaber, S. H. L. Austin, M. D. M. Masdeu, A. Edwards, N. Urbán, A. Marciniak-Czochra, F. Guillemot, Coordinated changes in cellular behavior ensure the lifelong maintenance of the hippocampal stem cell population. *Cell Stem Cell* **28**, 863–876.e6 (2021). doi:10.1016/j.stem.2021.01.003 Medline

13. S. Sultan, L. Li, J. Moss, F. Petrelli, F. Cassé, E. Gebara, J. Lopatar, F. W. Pfrieger, P. Bezzi, J. Bischofberger, N. Toni, Synaptic Integration of Adult-Born Hippocampal Neurons Is Locally Controlled by Astrocytes. *Neuron* **88**, 957–972 (2015). doi:10.1016/j.neuron.2015.10.037 Medline

14. A. Sierra, J. M. Encinas, J. J. Deudero, J. H. Chancey, G. Enikolopov, L. S. Overstreet-Wadiche, S. E. Tsirka, M. Maletic-Savatic, Microglia shape adult hippocampal neurogenesis through apoptosis-coupled phagocytosis. *Cell Stem Cell* **7**, 483–495 (2010). doi:10.1016/j.stem.2010.08.014 Medline

15. T. D. Palmer, A. R. Willhoite, F. H. Gage, Vascular niche for adult hippocampal neurogenesis. *J. Comp. Neurol.* **425**, 479–494 (2000). doi:10.1002/1096-9861(20001002)425:4<479:AID-CNE2>3.0.CO;2-3 Medline

16. Z. Liu, L. J. Martin, The adult neural stem and progenitor cell niche is altered in amyotrophic lateral sclerosis mouse brain. *J. Comp. Neurol.* **497**, 468–488 (2006). doi:10.1002/cne.21012 Medline

17. F. Christidi, E. Karavasilis, M. Rentzos, G. Velonakis, V. Zouvelou, S. Xirou, G. Argyropoulos, I. Papatriantafyllou, V. Pantolewn, P. Ferentinos, N. Kelekis, I. Seimenis, I. Evdokimidis, P. Bede, Hippocampal pathology in amyotrophic lateral sclerosis: Selective vulnerability of subfields and their associated projections. *Neurobiol. Aging* **84**, 178–188 (2019). doi:10.1016/j.neurobiolaging.2019.07.019 Medline

18. K. L. Harris, M. Armstrong, R. Swain, S. Erzinclioglu, T. Das, N. Burgess, R. A. Barker, S. L. Mason, Huntington's disease patients display progressive deficits in hippocampal-dependent cognition during a task of spatial memory. *Cortex* **119**, 417–427 (2019). doi:10.1016/j.cortex.2019.07.014 Medline

19. J. Terreros-Roncal, M. Flor-García, E. P. Moreno-Jiménez, N. Pallas-Bazarra, A. Rábano, N. Sah, H. van Praag, D. Giacomini, A. F. Schinder, J. Ávila, M. Llorens-Martín, Activity-Dependent Reconnection of Adult-Born Dentate Granule Cells in a Mouse Model of Frontotemporal Dementia. *J. Neurosci.* **39**, 5794–5815 (2019). doi:10.1523/JNEUROSCI.2724-18.2019 Medline

20. L. Walker, L. Stefanis, J. Attems, Clinical and neuropathological differences between Parkinson's disease, Parkinson's disease dementia and dementia with Lewy bodies - current issues and future directions. *J. Neurochem.* **150**, 467–474 (2019). doi:10.1111/jnc.14698 Medline

21. M. Bocchetta, J. E. Iglesias, M. A. Scelsi, D. M. Cash, M. J. Cardoso, M. Modat, A. Altmann, S. Ourselin, J. D. Warren, J. D. Rohrer, Hippocampal Subfield Volumetry: Differential Pattern of Atrophy in Different Forms of Genetic Frontotemporal Dementia. *J. Alzheimers Dis.* **64**, 497–504 (2018). doi:10.3233/JAD-180195 Medline

22. S. Abdulla, J. Machts, J. Kaufmann, K. Patrick, K. Kollewe, R. Dengler, H. J. Heinze, S. Petri, S. Vielhaber, P. J. Nestor, Hippocampal degeneration in patients with amyotrophic lateral sclerosis. *Neurobiol. Aging* **35**, 2639–2645 (2014). doi:10.1016/j.neurobiolaging.2014.05.035 Medline

23. M. A. Curtis, E. B. Penney, A. G. Pearson, W. M. van Roon-Mom, N. J. Butterworth, M. Dragunow, B. Connor, R. L. Faull, Increased cell proliferation and neurogenesis in the adult human Huntington's disease brain. *Proc. Natl. Acad. Sci. U.S.A.* **100**, 9023–9027 (2003). doi:10.1073/pnas.1532244100 Medline

24. G. U. Höglinger, P. Rizk, M. P. Muriel, C. Duyckaerts, W. H. Oertel, I. Caille, E. C. Hirsch, Dopamine depletion impairs precursor cell proliferation in Parkinson disease. *Nat. Neurosci.* **7**, 726–735 (2004). doi:10.1038/nn1265 Medline

25. H. Konishi, T. Okamoto, Y. Hara, O. Komine, H. Tamada, M. Maeda, F. Osako, M. Kobayashi, A. Nishiyama, Y. Kataoka, T. Takai, N. Udagawa, S. Jung, K. Ozato, T. Tamura, M. Tsuda, K. Yamanaka, T. Ogi, K. Sato, H. Kiyama, Astrocytic phagocytosis is a compensatory mechanism for microglial dysfunction. *EMBO J.* **39**, e104464 (2020). doi:10.15252/embj.2020104464 Medline

26. J. K. Young, Neurogenesis Makes a Crucial Contribution to the Neuropathology of Alzheimer's Disease. *J. Alzheimers Dis. Rep.* **4**, 365–371 (2020). doi:10.3233/ADR-200218 Medline

27. P. Martínez-Martín, J. Avila; AD Research Unit Investigators, Alzheimer Center Reina Sofia Foundation: Fighting the disease and providing overall solutions. *J. Alzheimers Dis.* **21**, 337–348 (2010). doi:10.3233/JAD-2010-101149 Medline

28. International Society for Biological and Environmental Repositories, 2012 best practices for repositories collection, storage, retrieval, and distribution of biological materials for research international society for biological and environmental repositories. *Biopreserv. Biobank.* **10**, 79–161 (2012). doi:10.1089/bio.2012.1022 Medline

29. H. Braak, E. Braak, Staging of Alzheimer's disease-related neurofibrillary changes. *Neurobiol. Aging* **16**, 271–278 (1995). doi:10.1016/0197-4580(95)00021-6 Medline

30. H. Braak, I. Alafuzoff, T. Arzberger, H. Kretzschmar, K. Del Tredici, Staging of Alzheimer disease-associated neurofibrillary pathology using paraffin sections and immunocytochemistry. *Acta Neuropathol.* **112**, 389–404 (2006). doi:10.1007/s00401-006-0127-z Medline

31. C. B. Saper, P. E. Sawchenko, Magic peptides, magic antibodies: Guidelines for appropriate controls for immunohistochemistry. *J. Comp. Neurol.* **465**, 161–163 (2003). doi:10.1002/cne.10858 Medline

32. M. Llorens-Martín, I. Torres-Alemán, J. L. Trejo, Pronounced individual variation in the response to the stimulatory action of exercise on immature hippocampal neurons. *Hippocampus* **16**, 480–490 (2006). doi:10.1002/hipo.20175 Medline

33. M. Bolós, M. Llorens-Martín, J. R. Perea, J. Jurado-Arjona, A. Rábano, F. Hernández, J. Avila, Absence of CX3CR1 impairs the internalization of Tau by microglia. *Mol. Neurodegener.* **12**, 59 (2017). doi:10.1186/s13024-017-0200-1 Medline

34. E. Sanchez-Mejias, V. Navarro, S. Jimenez, M. Sanchez-Mico, R. Sanchez-Varo, C. Nuñez-Diaz, L. Trujillo-Estrada, J. C. Davila, M. Vizuete, A. Gutierrez, J. Vitorica, Soluble phospho-tau from Alzheimer's disease hippocampus drives microglial degeneration. *Acta Neuropathol.* **132**, 897–916 (2016). doi:10.1007/s00401-016-1630-5 Medline

ACKNOWLEDGMENTS

The authors thank the patients and their families for generously donating brain samples. Moreover, they wish to thank I. Rodal, E. Hitt, and L. Saiz for their help with human sample extraction and processing, the Confocal Microscopy Facility at the CBMSO for their technical assistance, Drs. B. Berninger and B. Márquez-Valadez for their critical discussion of the data and help with manuscript preparation, and Enrique Terreros for his support with the design of Excel Macros. A number of human samples were generously provided by the Biobanco del Hospital Universitario Reina Sofia (Córdoba, Spain). The

authors express their thanks to Dr. R Sánchez for providing some of such samples. Requests for the prospective collection of equivalent brain samples will be fulfilled by Dr. Alberto Rábano under a material transfer agreement with the CIEN Foundation. **Funding:** European Research Council (ERC) (ERC-CoG-2020-101001916 (MLLM). Spain's Ministry of Economy and Competitiveness (PID2020-113007RB-I00, SAF-2017-82185-R and RYC-2015-171899 (MLLM). The Alzheimer's Association (2015-NIRG-340709, AARG-17-528125, and AARG-17-528125-RAPID) (MLLM). The Association for Frontotemporal Degeneration [2016 Basic Science Pilot Grant Award (MLLM)]. Center for Networked Biomedical Research on Neurodegenerative Diseases (CIBERNED, Spain) (MLLM). Institutional grants from the Fundación Ramón Areces and Banco de Santander to CBMSO are also acknowledged. The salary of JTR was supported by a Doctoral fellowship from the Universidad Autónoma de Madrid (FPI-UAM 2017 program). The salary of EPMJ was supported by a 2018 Neuroscience Doctoral fellowship from the Fundación Tatiana Pérez de Guzmán. The salary of MFG was supported by a Formación de Personal Investigador (FPI) contract, associated with the SAF-2017-82185-R grant (MLLM), supported by the Spain's Ministry for Economy and Competitiveness (PRE2018-085233). The salary of CBRM is supported by "Subvenciones para la promoción de empleo joven e Implantación de la garantía juvenil en I+D+i 2018" (PEJ2018-001725-A) awarded by the Spain's Ministry of Economy and Competitiveness to MLLM. **Author contributions:** Conceptualization: JTR, EPMJ, MFG, AR, MLLM. Data curation: JTR, MLLM. Formal Analysis: JTR, EPMJ, MFG, CBRM, FC, MLLM. Funding acquisition: MLLM. Investigation: JTR, EPMJ, MFG, CBRM, AR, FC, MLLM. Methodology: JTR, EPMJ, MFG, CBRM, AR, MLLM. Project administration: MLLM. Resources: AR, LLM. Supervision: MLLM. Validation: JTR, EPMJ, MFG, AR, MLLM. Visualization: JTR, EPMJ, MFG, AR, MLLM. Writing – original draft: MLLM. Writing – review and editing: JTR, EPMJ, MFG, CBRM, AR, MFT, FC, MLLM. **Competing interests:** Authors declare no competing interests. **Data and materials availability:** All data are available in the main text or the supplementary materials.

SUPPLEMENTARY MATERIALS

science.org/doi/10.1126/science.abl5163
Materials and Methods
Figs. S1 to S17
Tables S1 to S3
References (*27*–*34*)
MDAR Reproducibility Checklist
Data S1 and S2

19 July 2021; accepted 6 October 2021
Published online 21 October 2021
10.1126/science.abl5163

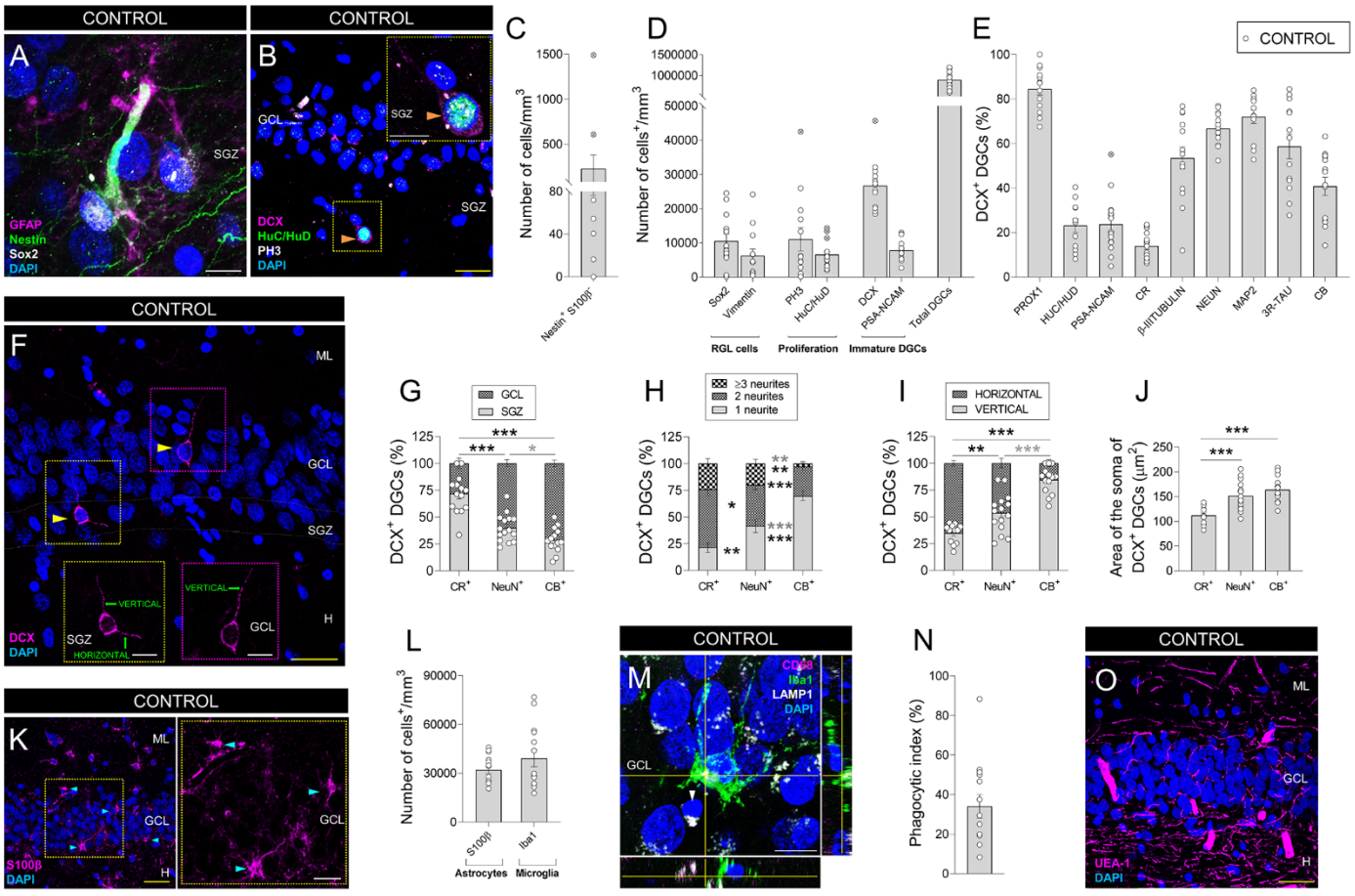

Fig. 1. Adult hippocampal neurogenesis in neurologically healthy control subjects. (**A** to **B**) Representative images of a Nestin$^+$ SRY-Box Transcription Factor 2 (Sox2)$^+$ glial fibrillary acidic protein (GFAP$^+$) radial glia-like (RGL) cell (A), and a Phospho-histone 3 (PH3)$^+$ HuC/HuD$^+$ Doublecortin (DCX)$^+$ proliferative neuroblast (B) in the human dentate gyrus (DG). (**C** to **D**) Density of Nestin$^+$ S100β$^-$ RGL cells (C), and Sox2$^+$, Vimentin$^+$, PH3$^+$, Huc/HuD$^+$ cells, DCX$^+$ and Polysialylated-neural cell adhesion molecule (PSA-NCAM)$^+$ immature and total dentate granule cells (DGCs) (D) in neurologically healthy control subjects. (**E**) Percentage of DCX$^+$ immature DGCs that express markers of distinct maturation stages. (**F**) Representative images showing morphologically undifferentiated (left) and differentiated (right) human DCX$^+$ immature DGCs. (**G**) Positioning of DCX$^+$ DGC subpopulations. (**H**) Number of primary neurites of DCX$^+$ DGCs. (**I**) Orientation of neurites in DCX$^+$ DGCs. (**J**) Area of the soma of DCX$^+$ DGCs. (**K**) Representative images of S100β$^+$ astrocytes. (**L**) Density of S100β$^+$ astrocytes and Iba1$^+$ microglia. (**M**) Representative image of an Iba1$^+$ microglial cell showing the presence of a phagocytic pouch in the proximity of a pyknotic nucleus in the human DG. (**N**) *Phagocytic index*. (**O**) Representative image showing the vascularization of the human DG. n = 15 neurologically healthy control subjects. In (A), (B), (F), (K), (M), and (O), Z-projection images are shown. 5 to 20 stacks of images per subject were analyzed for each marker. Graphs represent mean values ± SEM. ML: Molecular layer. GCL: Granule cell layer. SGZ: Subgranular zone. H: Hilus. CR: Calretinin. CB: Calbindin. Yellow scale bar: 50 μm. White scale bar: 10 μm. Orange triangles: PH3$^+$ HuC/HuD$^+$ DCX$^+$ cells. Yellow triangles: DCX$^+$ DGCs. Blue triangles: S100β$^+$ astrocytes. White triangle: pyknotic nucleus. *0.05 > *P* ≥ 0.01; **0.01 > *P* ≥ 0.001; and ***P <0.001. Black asterisks indicate changes with respect to DCX$^+$ CR$^+$ DGCs. Gray asterisks indicate changes between DCX$^+$ NeuN$^+$ and DCX$^+$ CB$^+$ DGCs. Crossed out dots in (C), (D), and (E) indicate outlier values.

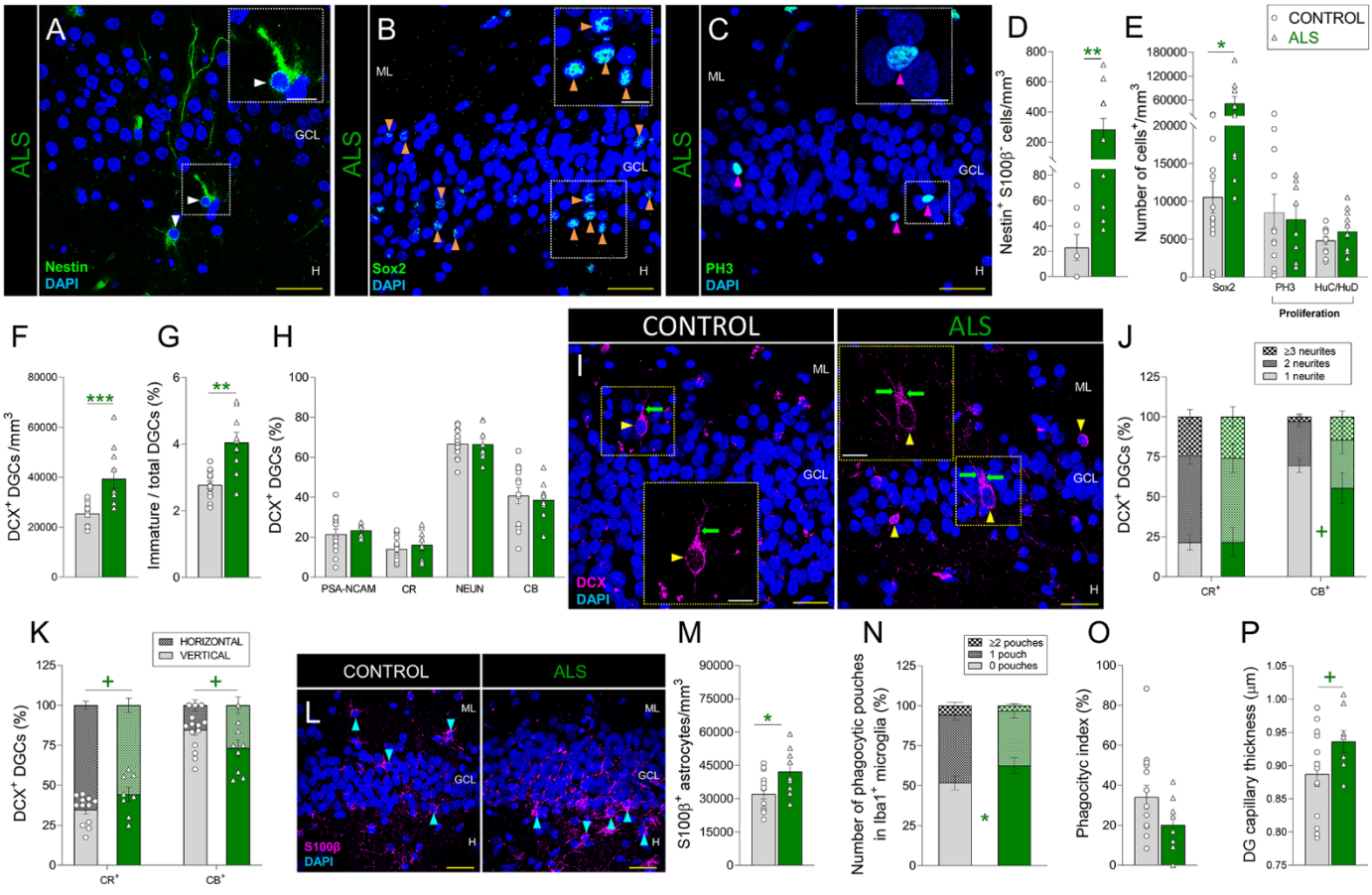

Fig. 2. Adult hippocampal neurogenesis in Amyotrophic lateral sclerosis (ALS). (**A** to **C**): Representative images of Nestin$^+$ (A), Sox2$^+$ (B), and Phospho-histone 3 (PH3)$^+$ cells (C). (**D** to **E**) Density of Nestin$^+$ S100β$^-$ radial glia-like cells (D), Sox2$^+$ cells, PH3$^+$ proliferative cells, and HuC/HuD$^+$ proliferative neuroblasts (E). (**F**) Density of Doublecortin (DCX)$^+$ immature dentate granule cells (DGCs). (**G**) Ratio between immature and total DGCs. (**H**) Percentage of DCX$^+$ immature DGCs that express markers of distinct maturation stages. (**I**) Representative images of DCX$^+$ immature DGCs showing the presence of apical dendrites (green arrows). (**J**) Number of primary neurites in DCX$^+$ DGCs. (**K**) Orientation of primary neurites in DCX$^+$ DGCs. (**L**) Representative images of S100β$^+$ astrocytes. (**M**) Density of S100β$^+$ astrocytes. (**N**) Number of phagocytic pouches in Iba1$^+$ microglia. (**O**) *Phagocytic index*. (**P**) Thickness of *Ulex Europaea* Agglutinin 1 (UEA-1)$^+$ dentate gyrus capillaries. n = 15 neurologically healthy control subjects and 12 patients with ALS. In (A to C), (I), and (L), Z-projection images are shown. 5 to 20 stacks of images per subject were analyzed for each marker. Graphs represent mean values ± SEM. ML: Molecular layer. GCL: Granule cell layer. SGZ: Subgranular zone. H: Hilus. CR: Calretinin. CB: Calbindin. Yellow scale bar: 50 μm. White scale bar: 10 μm. White triangles: Nestin$^+$ RGL cells. Orange triangles: Sox2$^+$ cells. Magenta triangles: PH3$^+$ cells. Yellow triangles: DCX$^+$ DGCs. Blue triangles: S100β$^+$ astrocytes. $^+$ $0.1 > P \geq 0.05$; * $0.05 > P \geq 0.01$; ** $0.01 > P \geq 0.001$; and *** $P < 0.001$. Green asterisks indicate changes with respect to neurologically healthy controls.

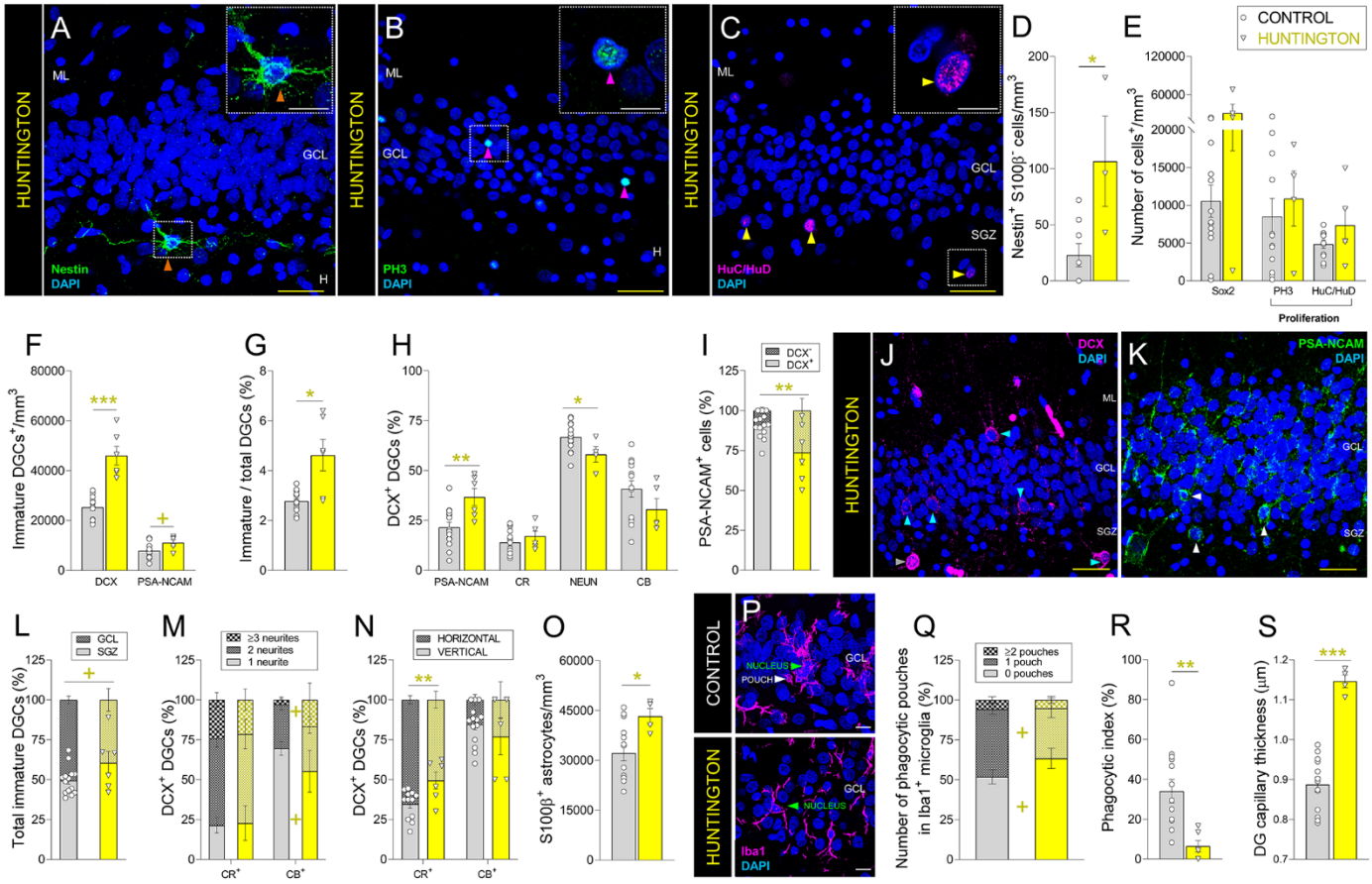

Fig. 3. Adult hippocampal neurogenesis in patients with Huntington's disease. (**A** to **C**) Representative images of Nestin$^+$ cells (A), Phospho-histone 3 (PH3)$^+$ proliferative cells (B), and HuC/HuD$^+$ proliferative neuroblasts (C). (**D** to **E**) Density of Nestin$^+$ S100β$^-$ radial glia-like cells (D), Sox2$^+$ cells, PH3$^+$ proliferative cells, and HuC/HuD$^+$ proliferative neuroblasts (E). (**F**) Density of Doublecortin (DCX)$^+$ and Polysialylated-neural cell adhesion molecule (PSA-NCAM)$^+$ immature dentate granule cells (DGCs). (**G**) Ratio between immature/total DGCs. (**H**) Percentage of DCX$^+$ immature DGCs that express markers of distinct maturation stages. (**I**) Percentage of PSA-NCAM$^+$ DGCs that express DCX. (**J** to **K**) Representative images of DCX$^+$ (J) and PSA-NCAM$^+$ (K) immature DGCs. (**L**) Positioning of immature DGCs. (**M**) Number of primary neurites of distinct subpopulations of DCX$^+$ DGCs. (**N**) Orientation of neurites in DCX$^+$ DGCs. (**O**) Density of S100β$^+$ astrocytes. (**P**) Representative images of Iba1$^+$ microglia. (**Q**) Number of phagocytic pouches in Iba1$^+$ microglia. (**R**) *Phagocytic index*. (**S**) Thickness of *Ulex Europaeus* Agglutinin 1 (UEA1)$^+$ dentate gyrus capillaries. n = 15 neurologically healthy control subjects and 6 patients with Huntington´s disease. In (A to C), (J to K), and P, Z-projection images are shown. 5 to 20 stacks of images per subject were analyzed for each marker. Graphs represent mean values ± SEM. ML: Molecular layer. GCL: Granule cell layer. SGZ: Subgranular zone. H: Hilus. CR: Calretinin. CB: Calbindin. Yellow scale bar: 50 μm. White scale bar: 10 μm. Orange triangles: Nestin$^+$ RGL cells. Magenta triangles: PH3$^+$ cells. Yellow triangles: HuC/HuD$^+$ cells. Blue triangles: DCX$^+$ immature DGCs. White triangles: PSA-NCAM$^+$ immature DGCs. $^+$ 0.1 > *P* ≥ 0.05; * 0.05 > *P* ≥ 0.01; ** 0.01 > *P* ≥ 0.001; and ***P < 0.001. Yellow asterisks indicate changes with respect to neurologically healthy controls.

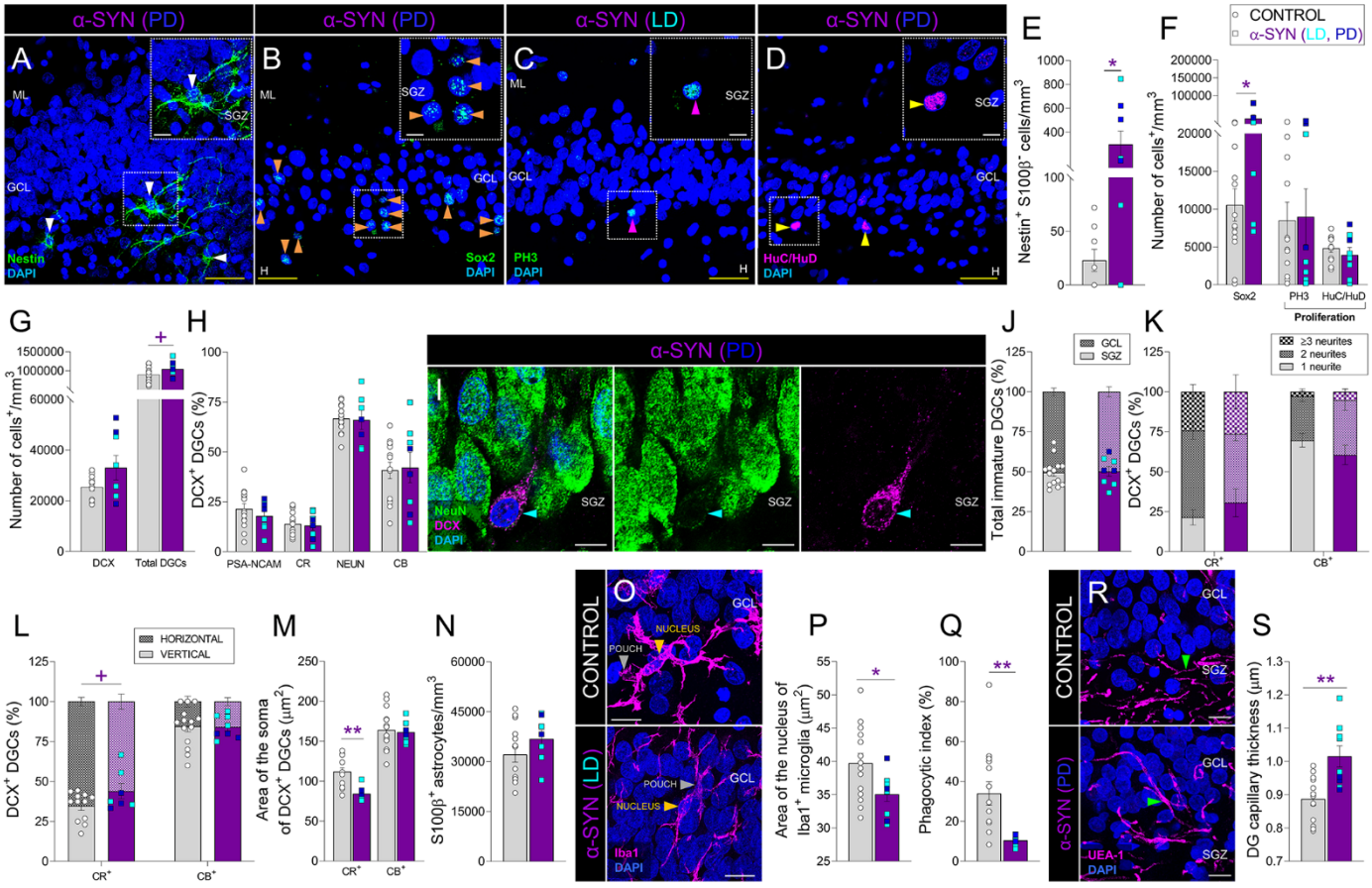

Fig. 4. Adult hippocampal neurogenesis in patients with α-synucleinopathies (α-SYN). (**A** to **D**) Representative images of Nestin$^+$ (A), Sox2$^+$ (B), Phospho-histone 3 (PH3)$^+$ cells (C), and HuC/HuD$^+$ proliferative neuroblasts (D). (**E** to **F**) Density of Nestin$^+$ S100β$^-$ radial glia-like cells (E), Sox2$^+$ cells, PH3$^+$ proliferative cells, and HuC/HuD$^+$ proliferative neuroblasts (F). (**G**) Density of Doublecortin (DCX)$^+$ and total dentate granule cells (DGCs). (**H**) Percentage of DCX$^+$ immature DGCs that express markers of distinct maturation stages. (**I**) Representative high-power magnification images of a DCX$^+$ DGC. (**J**) Positioning of immature DGCs. (**K**) Number of primary neurites of distinct subpopulations of DCX$^+$ DGCs. (**L**) Neurite orientation in DCX$^+$ DGCs. (**M**) Area of the soma of DCX$^+$ DGCs. (**N**) Density of S100β$^+$ astrocytes. (**O**) Representative images of Iba1$^+$ microglia. (**P**) Area of the nucleus of Iba1$^+$ microglia. (**Q**) *Phagocytic index*. (**R**) Representative images showing the vascularization of the dentate gyrus (DG). (**S**) Thickness of *Ulex Europaeus* Agglutinin 1 (UEA-1)$^+$ DG capillaries. n = 15 neurologically healthy control subjects and 9 patients with α-SYN [3 with Parkinson's disease (PD) and 6 with dementia with Lewy bodies (LD)]. In (A to D), (I), (O), and (R), Z-projection images are shown. 5 to 20 stacks of images per subject were analyzed for each marker. Graphs represent mean values ± SEM. ML: Molecular layer. GCL: Granule cell layer. SGZ: Subgranular zone. H: Hilus. CR: Calretinin. CB: Calbindin. Yellow scale bar: 50 μm. White scale bar: 10 μm. White triangles: Nestin$^+$ RGL cells. Orange triangles: Sox2$^+$ cells. Magenta triangles: PH3$^+$ cells. Yellow triangles: HuC/HuD$^+$ cells. Blue triangles: DCX$^+$ immature DGCs. Green triangles: UEA1$^+$ capillaries. $^+$ 0.1 > *P* ≥ 0.05; * 0.05 > *P* ≥ 0.01; ** 0.01 > *P* ≥ 0.001; and ****P* < 0.001. Purple asterisks indicate changes with respect to neurologically healthy controls.

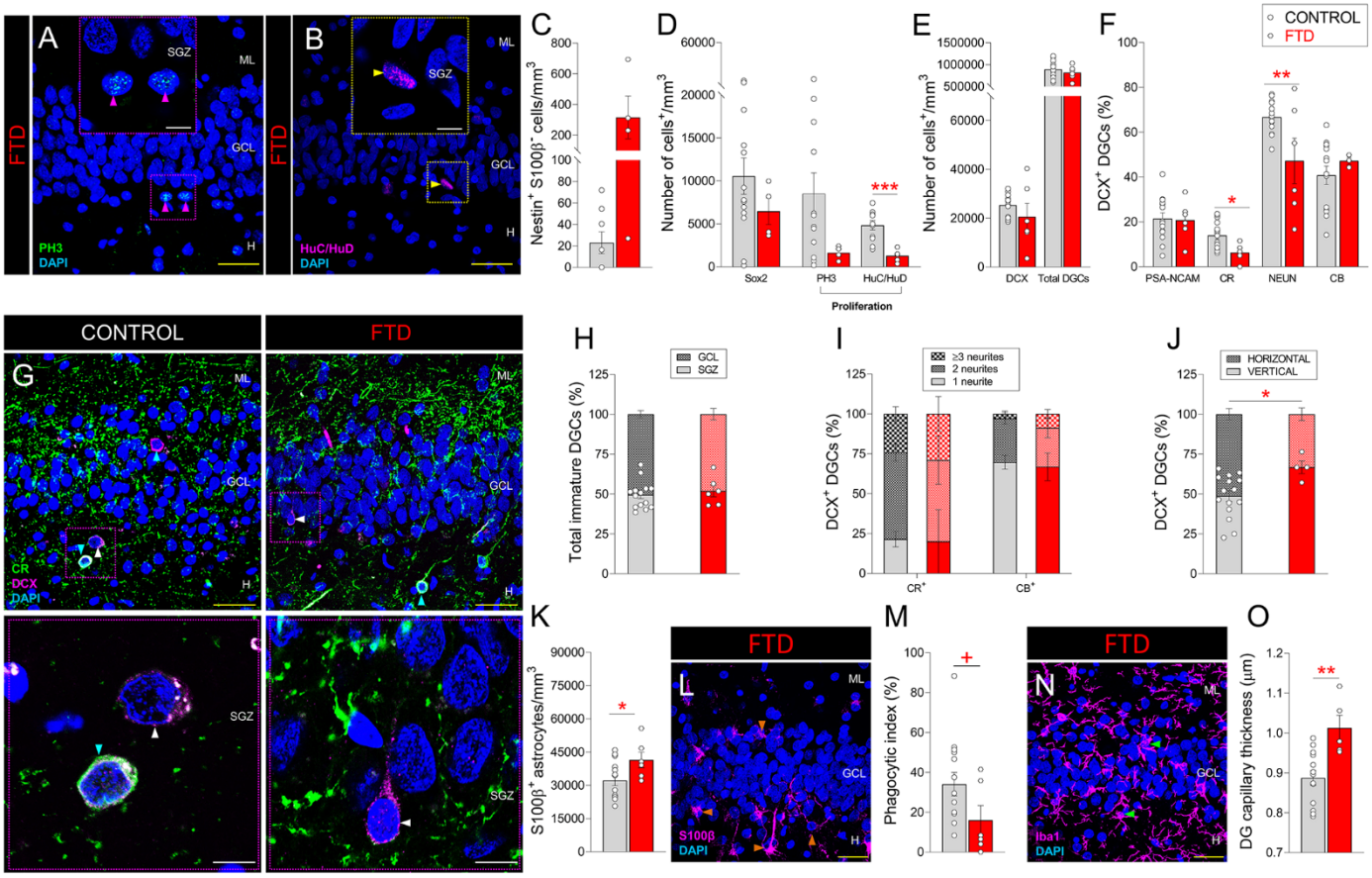

Fig. 5. Adult hippocampal neurogenesis in Frontotemporal dementia (FTD). (**A** to **B**) Representative images of Phospho-histone 3 (PH3)$^+$ proliferative cells (A) and HuC/HuD$^+$ proliferative neuroblasts (B) in patients with FTD. (**C to D**) Density of Nestin$^+$ S100β$^-$ radial glia-like cells (C), Sox2$^+$ cells, PH3$^+$ proliferative cells, and HuC/HuD$^+$ proliferative neuroblasts (D). (**E**) Density of DCX$^+$ and total dentate granule cells (DGCs). (**F**) Percentage of DCX$^+$ immature DGCs that express markers of distinct maturation stages. (**G**) Representative low- and high-power magnification images of Doublecortin (DCX)$^+$ DGCs. (**H**) Positioning of total immature DGCs. (**I**) Number of neurites in DCX$^+$ DGCs. (**J**) Neurite orientation in DCX$^+$ DGCs. (**K**) Density of S100β$^+$ astrocytes. (**L**) Representative images of S100β$^+$ astrocytes. (**M**) *Phagocytic index*. (**N**) Representative images of Iba1$^+$ microglia. (**O**) Thickness of *Ulex Europaeus* Agglutinin 1 (UEA-1)$^+$ dentate gyrus capillaries. n = 15 neurologically healthy control subjects and 6 patients with FTD. In (A to B), (G), (L), and (N), Z-projection images are shown. 5 to 20 stacks of images per subject were analyzed for each marker. Graphs represent mean values ± SEM. ML: Molecular layer. GCL: Granule cell layer. SGZ: Subgranular zone. H: Hilus. CR: Calretinin. CB: Calbindin. Yellow scale bar: 50 μm. White scale bar: 10 μm. Magenta triangles: PH3$^+$ cells. Yellow triangles: HuC/HuD$^+$ cells. Blue triangles: DCX$^+$ CR$^+$ immature DGCs. White triangles: DCX$^+$ CR$^-$ immature DGCs. Orange triangles: S100β$^+$ astrocytes. Green triangles: Iba1$^+$ microglia. $^+$ $0.1 > P \geq 0.05$; * $0.05 > P \geq 0.01$; ** $0.01 > P \geq 0.001$; and *** $P < 0.001$. Red asterisks indicate changes with respect to neurologically healthy controls.

A

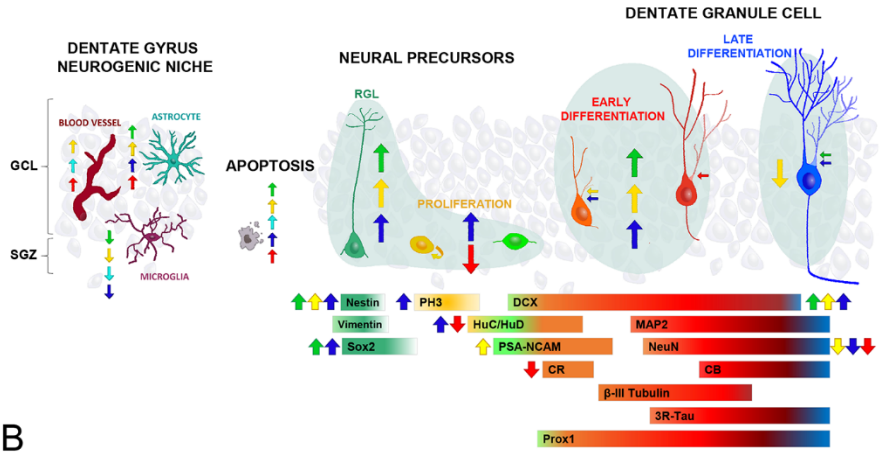

B

			α- SYNUCLEOINOPATHIES		
	ALS	HUNTINGTON	LEWY	PARKINSON	FTD
DENTATE GYRUS NEUROGENIC NICHE					
Astrocytes	↑	↑	=	↑	↑
Microglia	↓ Phagocytic pouches	↓ *Phagocytic index*	↓ Nucleus size ↓ *Phagocytic index*	↓ Phagocytic pouches	=
Vasculature	=	↑	↑	=	↑
APOPTOSIS					
Pyknotic cells	↑	↑	↑	↑	↑
NEURAL PRECURSORS					
RGL cells	↑	↑	=	↑	=
Proliferation	=	=	=	↑	↓
DENTATE GRANULE CELLS					
Immature DGCs	↑	↑	=	↑	=
Morphological maturation	Tendency to be altered	Altered	Altered	Altered	Altered
Differentiation (marker expression)	=	Altered	=	Altered	Altered
Total DGCS	=	↑	=	=	=

Fig. 6. Adult hippocampal neurogenesis (AHN) in neurodegenerative diseases. (**A**) Graphical scheme showing the stages of AHN targeted by each neurodegenerative disease. (**B**) Summary of the main alterations found in each disease.

Impact of neurodegenerative diseases on human adult hippocampal neurogenesis

J. Terreros-RoncalE. P. Moreno-JiménezM. Flor-GarcíaC. B. Rodríguez-MorenoM. F. TrincheroF. CafiniA. RábanoM. Llorens-Martín

Science, **Ahead of Print**